SANDIA REPORT

SAND2011-9417
Unlimited Release
December 2011

Membranes and Surfaces Nano-engineered for Pathogen Capture and Destruction

May D. Nyman and Tom A. Stewart

Prepared by
Sandia National Laboratories
Albuquerque, New Mexico 87185 and Livermore, California 94550

Sandia National Laboratories is a multi-program laboratory managed and operated by Sandia Corporation, a wholly owned subsidiary of Lockheed Martin Corporation, for the U.S. Department of Energy's National Nuclear Security Administration under contract DE-AC04-94AL85000.

Issued by Sandia National Laboratories, operated for the United States Department of Energy by Sandia Corporation.

Available to DOE and DOE contractors from
U.S. Department of Energy
Office of Scientific and Technical Information
P.O. Box 62
Oak Ridge, TN 37831

Telephone: (865)576–8401
Facsimile: (865)576–5728
E–Mail: reports@adonis.osti.gov
Online ordering: http://www.doe.gov/bridge

Available to the public from
U.S. Department of Commerce
National Technical Information Service
5285 Port Royal Rd
Springfield, VA 22161

Telephone: (800)553–6847
Facsimile: (703)605–6900
E–Mail: orders@ntis.fedworld.gov
Online order: http://www.ntis.gov/ordering.htm

SAND2011-9417
Unlimited Release
December 2011

Membranes and Surfaces Nano-engineered for Pathogen Capture and Destruction

May Nyman and Tom Stewart

Geochemistry Department
Sandia National Laboratories
P.O. Box 5800
Albuquerque, NM 87185–0754

ABSTRACT

This project (LDRD 130749) addressed the fundamentals of capturing water-borne pathogens on a surface, and their destruction by photocatalytic processes. Microbiological pathogens, viruses and bacteria in particular, are of great concern in municipal and at-the-source water supplies, particularly as these sources become scarcer and more polluted with increasing population coupled with increasing industrialization of developing countries. Filtration (over coagulation for instance) remains a method of choice for water treatment for both municipal plants and at-the-source or home treatment, given the ease of use, rapid treatment rate, and re-usability filter media (thus reduced cost). However, size-exclusion filtration is challenging for small pathogens such as viruses. Therefore filtration by chemical affinity is an attractive option. Self-cleaning membranes or surfaces are also particularly attractive for water treatment technologies, in that biofouling is a considerable challenge. Furthermore, the ability to clean filtration media extends its use and lifetime.

We have explored three general themes in this project: 1) Screening chemical surface modifiers for pathogen capture, 2) Developing photocatalysts and 3) Combining both on surfaces to demonstrate capture followed by photocatalytic destruction. Pathogen capture was done most effectively by inorganic polycations, similar to active ingredients in coagulation reagents for water treatment. Furthermore they offered photodegradation resistance, which is problematic for comparably effective organic functional groups. We identified delaminated titanates as effective photocatalysts that could be readily attached to surfaces. Furthermore, we developed a cheap and time-effective method of synthesizing these. Combined on a surface, these showed synergistic functionality of capturing bacteriophage, followed by photocatalytic destruction.

This page is intentionally left blank

ACKNOWLEDGEMENTS

This work was funded by the LDRD program, project 130749.

This page is intentionally left blank

CONTENTS

LIST OF FIGURES

This page is intentionally left blank

1 INTRODUCTION

Fresh water supplies are becoming alarmingly scarce in the face of a growing population that demands a high standard of living. Water availability is impacted by both increased discharge of waste into the environment and faster depletion of clean, subsurface sources. In response, it is projected that wastewater reuse (gallons/yr) will necessarily double by 2035. Impaired water such as wastewater requires due diligence for removal of disease-causing pathogens; again, due to increased and concentrated anthropogenic contaminants. While filtration or coagulation/filtration is the most commonly used technology for wastewater treatment, it is not optimal or cost-effective for the demanding task of converting wastewater to potable water. The primary issues relative to microbiological contaminants are 1) Viruses are virtually impossible to filter by size exclusion due to their small diameter, and 2) Biofouling of membranes is a ubiquitous problem, regardless of the type of water that is treated. Finally, the public is wary of using tap water, let alone treated waste-water; due to infamous incidents such as the 1993 Milwaukee cryptosporidium outbreak, as well as general mistrust in local municipalities. However, confidence would build with development of highly effective, state-of-the-art treatment technologies.

We propose to address the problem of filtration of small pathogens utilizing nano-engineered filtration membranes or filtration media such as sand. The nano-engineered surface is functionalized with two main components: one component has an affinity for micro-organism capture, and the second component catalyzes destruction of micro-organisms including viruses and biofilm-generating bacteria, and releases the organic byproducts via controlled UV-initiation. Pathogen capture by chemical affinity rather than size exclusion will allow use of larger-pore membranes, thus eliminating problems related to very small pores including high pressure (and energy) requirements to force the water through the membrane, pore clogging, and slow filtration rate. Furthermore, if filtration through a membrane or filter bed removes pathogens with greater confidence, chemical treatment such as chlorination may not be required in some cases. Chlorination, though cheap and widely used has the drawback of introducing soluble chlorocarbons into the water. Pathogen destruction that can be manually initiated will allow for controlled cleaning to minimize biofouling, increase the lifetime of filtration media, decrease operation costs, increase efficiency of water treatment processes, and gain public confidence. These goals help ensure a viable future for wastewater treatment technologies, and thus mitigate the world-wide growing water crisis.

This page is intentionally left blank

2 FUNCTIONALIZED SURFACES FOR CHEMICAL AFFINITY OF MICROBES

2.1 Overview

In this section, we screen chemical functional groups for modification of surfaces in order to enhance chemical filtration of small microbes (i.e. viruses), as an alternative to size-exclusion filtration. Size-exclusion filtration becomes increasingly challenging with viruses, which are typically smaller than 50 nm in diameter. Challenges include increased pressure necessary to force water through small pores and increased potential for physical damage of filtration media as a result of the necessity of increased water pressure. Therefore, we need to consider surface functionalization groups that can attract and bind these small microbes by chemical affinity rather than size-exclusion. **Figure 1** illustrates the concept of size-exclusion filtration that is enhanced by functional groups for filtration via chemical affinity. Additional criteria for such functional groups include: 1) a method for attachment to a surface; 2) stability on that surface in aqueous conditions (i.e. does not readily detach); 3) stability in a range of common aqueous conditions encountered in potable water including pH (~6-8), ionic strength of the solution, and miscellaneous dissolved ions such as silica, phosphorous, $Ca2^{+}$, Mg^{2+}, Fe^{3+}, etc; 4) stability against photodegradation that will be performed by the attached photocatalyst, designed to destroy the adsorbed microbe.

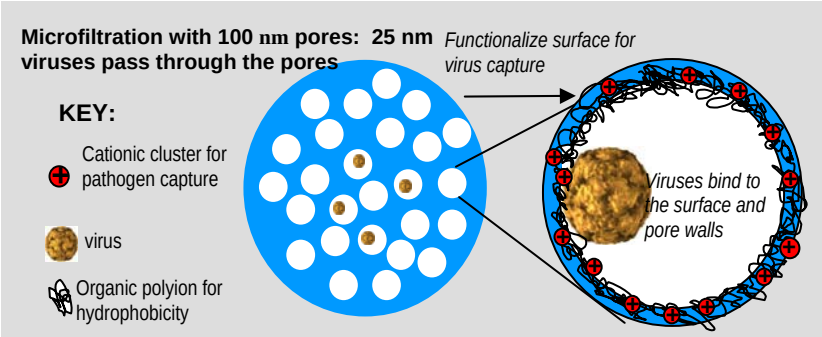

Figure 1. Illustration depicting chemical modification of a membrane surface for pathogen capture via chemical affinity rather than size exclusion.

For this study, we chose to utilize cationic function groups, since most microbes including viruses are anionic; and therefore the chemical affinity would be electrostatic. We investigated both organic and inorganic functional groups. The organic functional groups were attached to the surfaces through silane coupling agents, and the inorganic functional groups were adsorbed simply via electrostatic self-assembly. We utilized small columns filled with glass beads that were functionalized by the chemical functional groups as our test bed. In this configuration, there are very large pores between the beads, and therefore should operate in a filtration scenario primarily by chemical affinity rather than any sort of size-exclusion. Finally, a 27 nm diameter bacteriophage, MS-2 was used as a model contaminant due to its small size, ease of use in BSL-1 laboratory, and its robustness in a variety of aqueous conditions.

2.2 Experimental

Columns. Filtration of MS2 bacteriophage using chemically modified surfaces was carried out in Pierce Spin Columns, which are autoclavable and have a bed volume of 2 mL (total capacity of 5 mL, catalog #P189896). These are dimensioned to sit inside standard centrifuge tubes, allowing loading and elution without pumps or tubing, using either gravity or centrifugation. The filtration medium and support for chemically-functionalized coatings was comprised of 0.5 mm diameter glass beads (Biospec). Before any coating procedure, the beads were cleaned with piranha, a 1:3 mixture of 30% hydrogen peroxide and concentrated sulfuric acid, for 4 hours, rinsed with deionized water, absolute methanol, deionized water, and dried at 100^{o}C under vacuum.

Coating filtration media
All silane coupling agents were purchased from Gelest, Inc, and these were used as received. Coating the beads with silane coupling agents was found to be most effective in a fresh mixture of absolute methanol, agent, and deionized water in volumetric proportions of 90:4:6, added in that order. Beads were exposed to the coating solution for 1-2 hours with continuous stirring, then placed on filter paper in a Buchner funnel for vacuum-assisted draining and cleaning. The beads were rinsed twice with absolute methanol and at least 10 volumes of deionized water (using water first proved to be detrimental). The coated and cleaned beads were then annealed for an hour at 90-100^{o}C, and were stored in a sealed glass container if not used right away. Secondary coatings, if applied (usually addition of a cationic metal (Al^{3+}, Ba^{2+}), were generally using aqueous solutions for one to two hours with stirring. Silane coupling agents (and their abbreviations) that were utilized include 1) aminopropylsilane (APS), 2) trimethyl-aminopropylsilane (TM-APS), 3) didecylmethl-aminopropylsilane (DDM-APS), 4) tributyl-aminopropylsilane (TB-APS), 5) diethylene-tri-aminopropylsilane (DE-TA-PS), 6) methyldisilane (MDS), and 7) benzyldisilane (BDS).

Aluminum polycations, $[(GeO_4)Al_{12}(OH)_{24}(H_2O)_{12}]^{8+}$ $[(AlO_4)Al_{12}(OH)_{24}(H_2O)_{12}]^{7+}$ and $[(GaO_4)Al_{12}(OH)_{24}(H_2O)_{12}]^{7+}$ (referred collectively as $MAl_{12}^{7/8+}$; M = Ge, Al, Ga) were synthesized as described prior, and used in the 'crude' form.(1) The solution was adjusted to about one pH point above their natural pH for a final pH of between 5 and 6, and the aluminum concentration was 900-1000 ppm, as determined by ICP-MS. Beads were first coated with methyldisilane, then rinsed with deionized water and dried before use, but not annealed again. We also applied analogous coating chemistries to glass slides, so that the coating could be characterized by UV-vis spectroscopy.

Column experiments. Dried, coated or control beads were loaded into the mini-columns at 2.5 grams each on the day of use. Air was displaced from the bed by adding deionized water, capping, inverting several times, and then allowing beads to settle under an excess of water. The beds were gravity-drained, then capped until needed. MS-2 containing solutions (10^5 pfu/ml concentration; pfu = plaque-forming unit) were added at 0.75 mL per column, a volume equal to the void volume of the settled bead bed, and allowed to reach equilibrium. One minute was allowed for binding, then elution was begun by first adding 0.25 mL of water, allowing it to sink in as eluate was captured in a centrifuge tube, followed by four more discrete additions of one

milliliter apiece as the eluate pool was collected. This solution was then plaque-assayed (see below) for MS-2 population, post column filtration experiment. **Figure 2a** shows an illustration of this procedure, and **figure 2b** illustrates a typical MS-2 plaque assay.

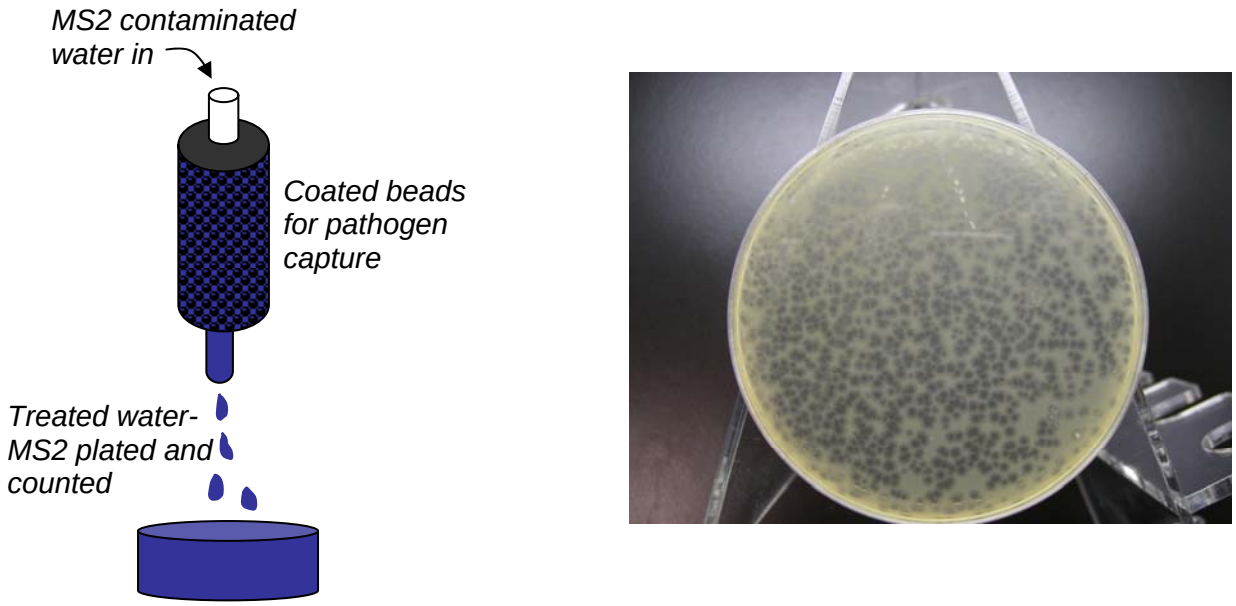

Figure 2. a) (left) illustration of the mini-column filtration experiments for chemical affinity filtration of MS-2 bacteriophage. b) (right) photograph of typical MS-2 plaque assay on E. Coli. Each dark spot represents a pfu (plaque-forming unit).

Cultivation of infectious agents. *Escherichia coli* strain C3000, the required host organism for the MS2 model virus, was obtained from American Type Culture Collection (ATCC) and maintained in continuous cultivation at 36±1^{o}C either in tryptic soy broth or on tryptic soy agar (TSA, 1.4% agar).

The MS2 bacteriophage used in viral clearance experiments was ATCC strain 15597-B1O, reconstituted from the freeze-dried state according to ATCC instructions and expanded into an early log-phase *E. coli* culture in order to produce a high-titer seed stock for routine use. Numbers of individual MS2 were visualized as plaque forming units (pfu) by dilution with sterile Dulbecco's phosphate buffered saline (DPBS) to a point where each live virus, when inoculated onto an agar plate of E. coli, would create a clarified zone (plaque) of infected and lysed bacteria.

For quantification, plaque assays were performed as described in the USEPA Manual of Methods for Virology.(2) Briefly, test samples were diluted in sterile DBSS, with a target of 100-300 pfu mL^{-1}, and combined with E. coli host cells in soft TSA (0.7% agar) at 44±1^{o}C. The molten mixture was spread onto a solid feeder layer of TSA in a 100 mm petri dish and allowed to gel. Plaques were counted after 14 to 16 hours of incubation. For virus removal experiments, the target MS2 load was typically 10^5 pfu per mini-column.

2.3 Results and Discussion

Correlation of surface coating with pathogen capture. We have focused on two main classes of surface chemistries: 1) Silanes with cationic functionalities, and 2) Metal-based cations and polycations anchored to aminosilanes or disilanes. Effect of hydrophilicity-hydrophobicity was also considered. See **figure 3** for a pictorial summary of surface chemistries and pathogen-binding affinities. The most effective of these amine-functionalized silanes is the triply-charged diethylene-triamino-propylsilane (DE-TA-PS). This is mostly likely due to its higher molecular charge. The three other amines vary in hydrophobicity with DDM-APS > TB-APS > TM-APS > APS. The MS2 removal efficacy matches this trend, indicating that hydrophibicity is a surface characteristic that also increase virus affinity. Furthermore, comparing the anionic controls, BDS (benzyldisilane) and MDS (methyldisilane) reveals the BDS actually has some binding affinity for MS-2, despite the fact that it carries a negative charge, while MDS captures negligible MS-2. The DE-TA-PS also can bind metals, so we modified this surface coating with addition of Fe^{3+}. While this did not increase the affinity for MS-2, it might for other microbes that utilize iron in metabolic processes. The MDS and BDS provided a second silane functionality for coupling to metal cations or polycations such as divalent Ba^{2+}, trivalent Al^{3+} and polycationic $[MAl_{12}O_4(OH)_{12}(H_2O)_{24}]^{7+}$ (M=Al,Ga). The anionic disilanes alone have minimal affinity for binding MS-2 at best. However, the addition of the metal cation or polycationic cluster produced various coatings with affinity for MS-2. The MDS-$GaAl_{12}$ is particularly effective, and thus chosen for further detailed studies in optimizing coating surface coating techniques. The BDS provides a functional group that adsorbs in the UV-vis for characterization purposes. In summary, these studies showed that both cationic charge and hydrophobicity are good surface characteristics for capturing anionic microbial contaminants such as MS-2. However, we also need to consider the stability of the coatings to UV-exposure for subsequential photocatalytic destruction of the adsorbed microbe. Therefore, all studies proceeded forward with the aluminum polycations. The much better MS-2 removal for $GaAl_{12}$ compared to $AlAl_{12}$ (Al_{13}) was somewhat puzzling initially. However, we attribute this to the poorer stability of Al_{13}, and its tendency to quickly aggregate into larger assemblies. Perhaps these larger assemblies do not strongly bind to the filtration surfaces, or they are easily removed, or they bind but are less effective due to decreased cationic charge-density. Thus these studies proceeded with $GaAl_{12}$ in particular.

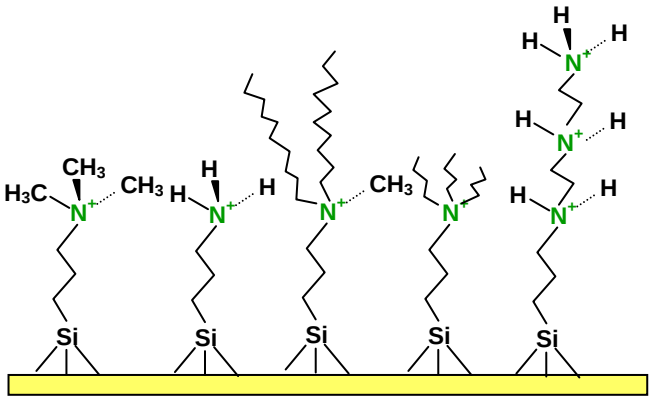

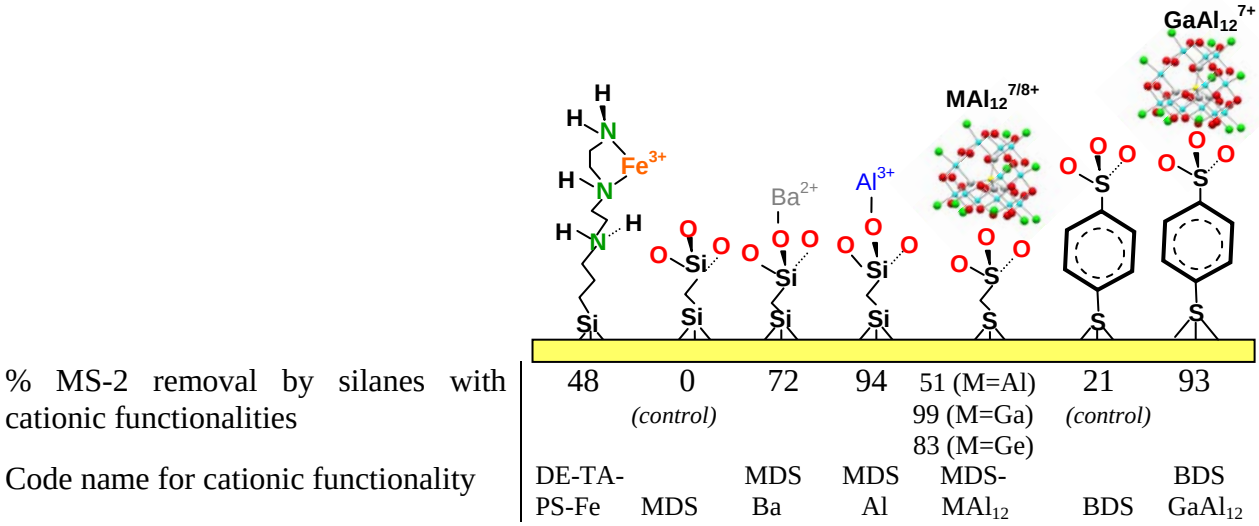

Figure 3. Pictorial representation of results of MS-2 filtration via chemically modified surfaces.

Characterization of surface coatings. One of the biggest challenges in developing nanoscale coatings on surfaces is finding direct methods of characterization, to prove that they are actually present, in that you generally cannot observe them directly. Indirectly, we can observe expected trend in MS-2 adsorption, but a direct characterization method is also desired. UV-vis spectroscopy is a possibility if the functional group is photoactive.(3) In this regard, we have pursued two routes for characterizing chemically modified surfaces by UV-vis spectroscopy, both utilizing multi-layer coatings. In both examples, the $GaAl_{12}^{7+}$ polycation is alternatively layered with an anionic photoactive specie, and multi-layered growth is monitored after each coating is applied. In one case, the photoactive specie is an anionic cluster of approximately the same size and shape as the aluminum polycation; phosphotungstate $[PW_{12}O_{40}]^{3-}$. The second is a polymer, polystyrene sulfonate. Illustrations of these multi-layer coatings of alternating anions and cations, along with the UV-vis spectra are shown in **figure 4**.

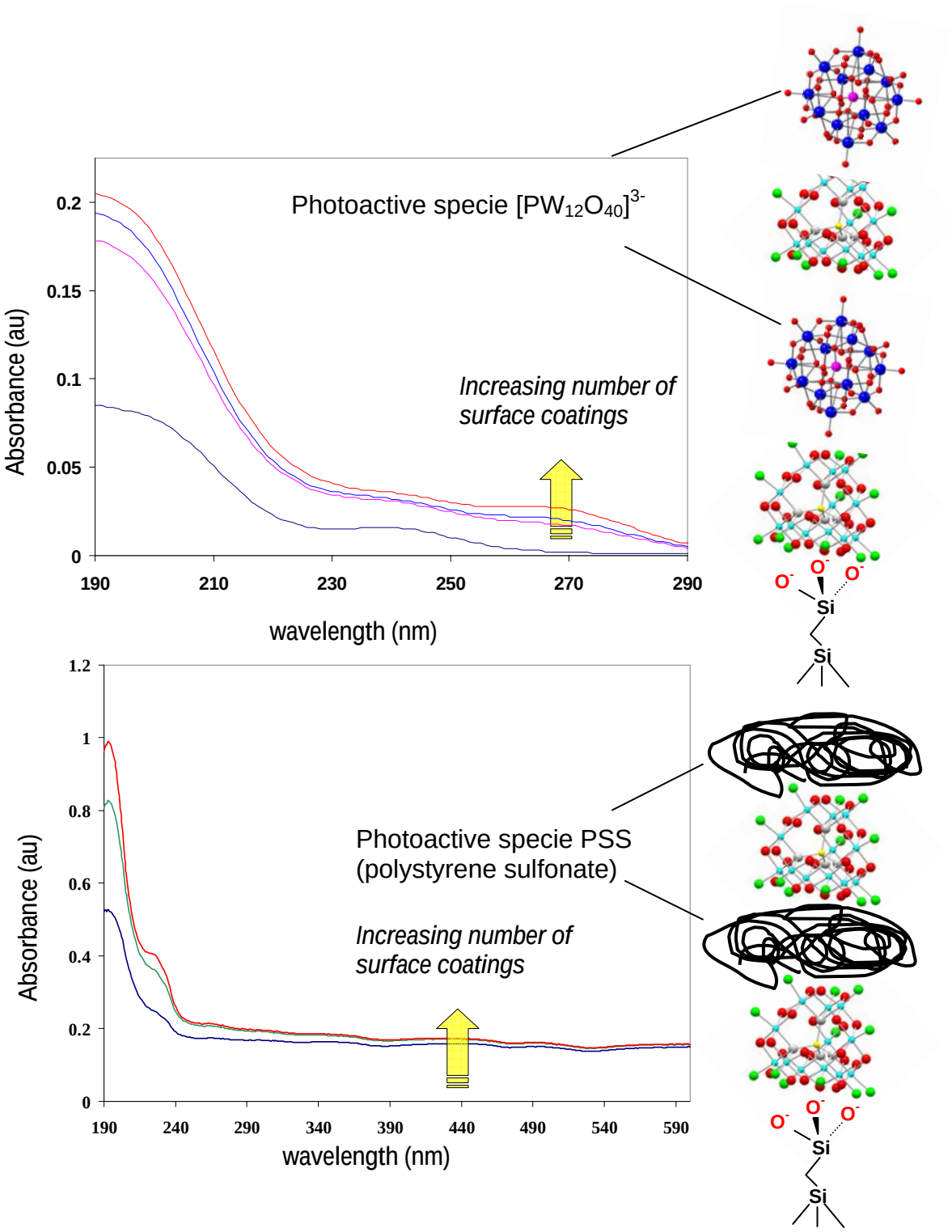

Figure 4. UV-vis spectra of multi-layer coating of $GaAl_{12}$ polycation interlayered with photoactive species to demonstrate a direct method of characterization of layer-by-layer surface coatings.

3 DEVELOPMENT OF PHOTOCATALYSTS

3.1 Background

In this section of the report we describe the development of photocatalysts that must possess the following criteria:

- Geometry conducive to surface coating
- Chemistry conducive to surface attachment
- Potent photocatalytic activity
- Compatibility with functionalities that adhere microbiological contaminants
- Economy and simplicity are also considered

Given these criteria, we found that coatings derived from titanate layers to be an optimal solution. Much of the results of these studies are summarized in a publication by Stewart et al.(**REF**); and this chapter is based on this publication.

In 1972, Fujishima and Honda reported that by irradiating a TiO_2 electrode with UV light, water splitting occurred via oxidation at the TiO_2 surface.(4) Since then, there has been an exponential growth in the development of TiO_2 and titanate photocatalytic materials, applications and devices. Applications include solar energy, degradation of contaminants (i.e. water treatment, self-cleaning surfaces), air-cleaning, and organic synthesis.(5-7) Optimization of titanate materials towards enhanced photocatalytic activity has been the focus of numerous studies: in particular, shifting the titanate band-gap into the visible spectrum, and introducing electron and/or hole traps for increased charge-separation have been targeted modifications. As a result of these studies, excellent titanate photocatalytic materials have been produced that are novel structures,(8, 9) doped,(10, 11) nanostructured,(12, 13) and incorporated into multi-functional composites.(14)

One particularly promising and simple class of Ti-based photocatalysts is the anionic delaminated titanate sheets, first reported by Sasaki and Watanabe in 1998.(15) These are formed from the layered lepidocrocite-like Cs-titanate material.(16) First the Cs^+ is exchanged for H^+,(17, 18) and then the titanate layers are exfoliated with large organic cations such as tetrabutylammonium (TBA^+).(15) The band-gap of these layers is 'blue-shifted' relative to TiO_2.(19) The titanate sheets are highly dispersible in water, and can be adsorbed onto a surface through electrostatic self-assembly as monolayers, or multi-layers alternating with cations.(20, 21) Although delamination of titanate layers was first reported over 10 years ago, photocatalytic investigations of the nanosheets are relatively limited in number. Methyl-blue and 2-propanol decomposition via titania nanosheets layered with polycation PDDA (poly-diallyldimethylammonium), as well as their annealed derivatives, has been demonstrated.(22) In another study, powders of titanate layers intercalated with polymerized polyanaline photo-

decomposed methyl-blue under visible light.(23) There have also been a few photocatalytic studies of the layered alkali titanates materials. Ide et al.(24) reported size-selective photocatalytic decomposition of benzene (from an aqueous mixture of benzene, phenol, and 4-butylphenol), based on the swelling of the interlayer space as a function of the alkali metal and its concentration relative to Ti in the layers. In another study,(25) the Cs-titanate was delaminated and then restacked with potassium cations, and the photocatalytic decomposition of methylene-blue was compared for the Cs^+-titanate, H^+-titanate and K^+-titanate. Higher surface area of the K^+-titanate material was suggested to be responsible for its superior performance. Also recently, photocatalytic water-splitting was investigated for K^+, TBA^+ and H^+ titanates.(26)

While the Cs-titanate parent material is usually synthesized by solid-state reactions and is a non-hydrous phase; a related layered sodium titanate material can be formed hydrothermally, known as sodium nonatitanate (SNT). SNT was originally described as $Na_4Ti_9O_{20}•xH_2O$,(27) and known for its ion-exchange properties and potential application in nuclear waste treatment.(28) Although the Cs:Ti ratio varies slightly for the Cs-titanate material, depending on the synthesis, an average formula is $Cs_{0.36}Ti_{0.91}O_2$.(17) Both structures have approximately double-layers of edge-sharing TiO_6 octahedra; the Cs-titanate has ~90% occupancy in the double-layers. The structure of the SNT has not been determined, due to its poorly crystalline nature. A major difference between the Cs-titanate and SNT is interlayer water that hydrates Na^+ in SNT, whereas the Cs-titanate contains no water. While delaminated Cs-titanate materials have been investigated as photocatalysts, the analogous delaminated SNT materials have not. Preparation, characterization and comparison of photocatalytic activity of delaminated titanate from SNT and Cs-titanate is one focus of this current study. We also prepared peroxide-modified, delaminated titanate sheets, where peroxide ligands replace some oxo and hydroxyl ligands, as indicated by the yellow color of these materials. It has been suggested that peroxide increases activity of TiO_2 photocatalysis, such as by repressing electron-hole recombination.(29) Peroxide ligation of titanate materials can also increase surface area as shown in ion sorption studies,(30) thereby also potentially providing enhancement for heterogeneous catalytic activity.

This study compares the methyl-orange and bromophenol blue photo-decomposition by four derivatives of delaminated titanates to each other, as well as to Degussa P25 ™ TiO_2. The four titanate catalysts are described as: 1) NaTi, 2) peroxide-NaTi, 3) CsTi and 4) peroxide-CsTi, which denote the parent material and peroxide ligation (or not).

3.2 Experimental

General Instrumentation and Characterization. For synthesis of the Cs-titanate, ion-exchange and delamination of the titanate materials, a Turbula® System Schatz WAB (Basel, Switzerland) was used for high-speed mechanical shaking. Generally, powders are placed in a 60 mL plastic tube with ~ 30 YSZ milling beads and 20-30 mL alcohol (i.e. methanol, isopropanol). The tube is capped tightly and sealed with electrical tape and mixed for 20-60 minutes. At various stages of their preparation, titanate materials are characterized by powder X-ray diffraction (XRD), thermogravimetry (TGA), infrared spectroscopy (IR). **Powder X-ray diffraction** was carried out on a Bruker D8 Advance diffractometer in Bragg-Brentano geometry with Cu-Kα radiation and a diffracted-beam graphite monochromator. **Infrared spectra, FTIR**, (400-4000 cm^{-1}) were recorded on a Thermo Nicolet 380 FT-IR equipped with a Smart Orbit (Diamond) ATR accessory. Thermal analysis was executed with a TA Instruments SDT 2960 for simultaneous thermogravimetric and differential thermal analysis (**TGA-DTA**) under air flow with a heating rate of 10 °C/min. High resolution transmission electron microscopy (**HR-TEM**) was utilized to characterize the size of the of the Degussa P25 ™ TiO_2 that provided a stable colloid suspension by processing in the Turbula (see below). HRTEM was done on a JEOL 2010 F with Gatan energy filtered imaging, in the High Resolution Microscope User Facility at UNM in Earth and Planetary Science Department.

Preparation of photocatalysts. The steps of photocatalyst preparation are summarized in **figure 5** and described below.

Synthesis of layered Cs-titanate. Using a procedure adapted from Sasaki,(17) we utilize a 1:2.65 ratio of Cs:Ti. TiO_2 (10 g, 0.125 mol) and Cs_2CO_3 (7.7 g, 0.047 mol Cs) were mixed as an alcohol slurry using the Turbula®. The alcohol was removed *in vacuo* with heating (40 °C) in a crucible, and the crucible with finely mixed, dry precursor powder was placed in an 800 °C oven overnight. Using the resulting powder, the mixing, drying and heating was repeated one time in order to obtain the pure desired phase (confirmed by XRD).

Synthesis of layered Na-nonatitanate (SNT). SNT was synthesized hydrothermally. Sodium hydroxide (NaOH; 10 g, 0.25 moles) was dissolve in 48 mL DI water in a 125-mL Teflon liner for a Parr reactor. Titanium (IV) isopropoxide (9.6 g, 0.033 moles) was added while stirring vigorously. A white slurry formed. The reactor was closed and placed in a 170°C oven for five days. Approximately 4 g of white powder product was collected by pressure filtration.

H^+-exchange of layered titanates. Proton exchange for Cs or Na was carried out with 1 molar HNO_3 solution, again utilizing the Turbula®. Several grams of alkali titanate were combined with 75 mL nitric acid in a Teflon bottle for this process. In these exchange conditions, neither layered phase is observed to undergo any dissolution. The H^+-exchanged powder was collected by centrifugation and washing; first with water then alcohol. Completeness of exchanged was checked by either energy dispersive spectroscopy (for Na or Cs), or thermogravimetry to 900 °C, followed by X-ray diffraction of the heat-treated powder. If Na or Cs remained, sodium titanate or cesium titanate phases would be observed in the diffraction pattern. If the Na or Cs was

completely removed, only TiO_2 was observed. The Cs-titanate required three acid-exchange steps, whereas the acid-exchange of SNT was completed in a single step.

Delamination of layered titanates. A 40 wt% tetrabutylammonium hydroxide (TBA) aqueous solution is diluted by ~50% with water; and the H^+-titanate powders are combined with the solution for Turbula® treatment for ~40 minutes. Again, the solid is isolated by centrifugation, washing and finally drying in a vacuum oven at 70 to 90 °C. Both materials only required one step for complete exchange.

Peroxide treatment of delaminated titanates. Dried titanates were ground to a fine powder with mortar and pestle, and suspended in 100% isopropanol at 0.5 wt.%. Hydrogen peroxide, 30% solution, was added dropwise with rapid stirring to a total of 2% of total volume, and allowed to react with continued stirring for 15 minutes. The yellowish peroxotitanates were separated from the mixture by repeated centrifugation and washing with isopropanol, and finally dried *in vacuo* at 70 to 90 °C.

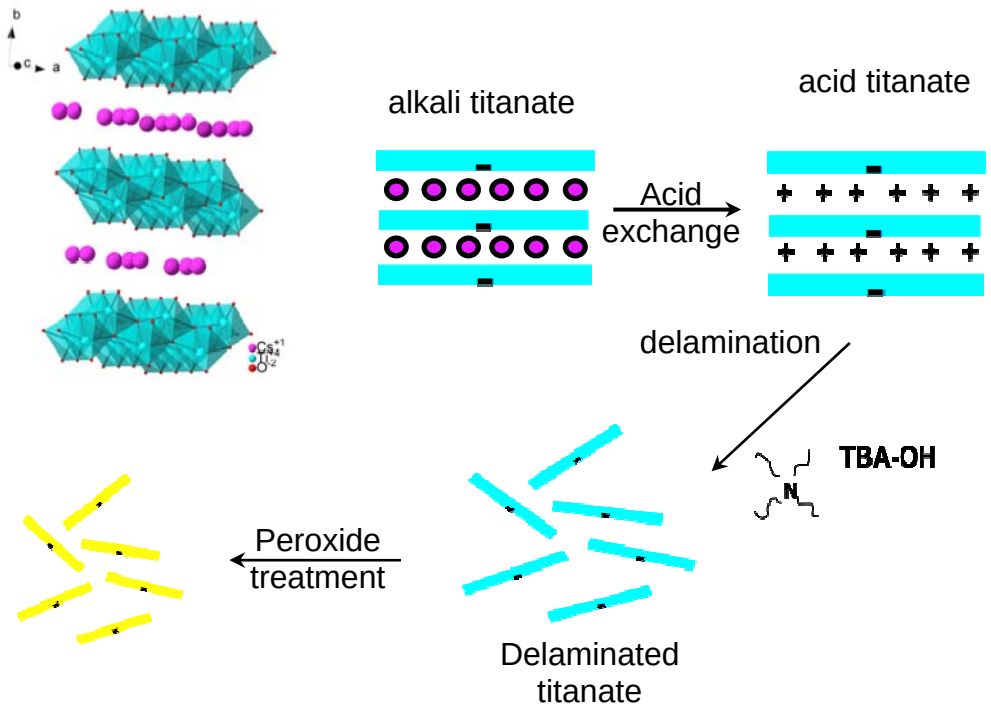

Figure 5. Schematic of the steps of titanate photocatalyst formation (see text). Blue layers are anionic titanate layers. Pink spheres are alkali cations (Na^+ or Cs^+), black '+' signs are H^+ cations. TBA-OH is tetramethylammonium cations [$(CH_3)_4N^+$]

UV-vis spectroscopy. was performed in either scanning (for characterization of titanate colloidal suspensions at concentrations of 20 μg/ml) or photometric mode (for quantifying dye concentrations) using a Shimadzu UV-3600 spectrophotometer and 1 cm quartz cuvettes.

Photocatalysis Experiments. The photon source was a germicidal lamp (GE model G15T8) with a radiant energy peak at 254 nm and overall irradiance rated as 49 mW/cm^2 at 2 cm distance. However, target solutions were held at 18 or 26 cm from the source in multiple 5-mL volumes, contained in 6-well, polystyrene plates (Nunc, Denmark, cat. no. 140675). In this way, up to twelve test articles could be exposed at once. **Figure 6** shows this experimental setup.

Figure 6. Photographs of experimental setup for UV-activated photodegradation of methyl-orange. Left is a view of the multi-well plates irradiated by an overhead UV-lamp. Wells can be set up to either screen different photocatalytic materials, or for time-dependant studies of a single material. Right shows increasing fading of the methyl-orange due to photocatalysis via delaminated titanates, with increasing experiment time from left to right

For most experiments, titanates were delivered in small volumes as colloidal suspensions created by shaking powdered preparations in deionized water with the Turbula® and YSZ beads, followed by centrifugation to remove all larger particles prone to settling. A colloidal suspension of Degussa P25 ™ TiO_2 (Aldrich) was prepared in the same way as were those of the delaminated titanates. A sample of each suspension was thoroughly dried and its residue weighed to calibrate concentrations.

Photocatalytic activity at low pH was investigated using methyl orange (MeO), typically at 0.5 or 1.0x10^{-5} molar concentration in pH 4.7 to 5.0, 0.01 M potassium phosphate buffer. Photocatalytic degradation of bromophenol blue (BrB) at 10^{-5} M concentration was usually carried out at pH 8.0 ±0.1 in 5 mM sodium borate buffer, although other buffers and concentrations were used at times. Final molar concentrations of the dyes were calculated from readings of absorption at either 480 nm or 590 nm for MO and BrB, respectively, using standard curves.

3.3 Results and Discussion

Preparation of titanate materials. Powder X-ray diffraction and infrared spectra of the delaminated titanates, NaTi and CsTi, from the SNT and Cs-titanate respectively looked very similar to both each other, as well as to similarly-prepared materials reported prior,(15, 26) see **figure 7**. **Figure 7a** shows X-ray diffraction spectra of original SNT and the TBA-delaminated SNT. Both are layered materials; the SNT has a d-spacing of ~10 Å, while the TBA-delaminated

has a layer-spacing of 17 Å. **Figure 7b** compared infrared spectra of both materials, clearly showing the vibrations of the TBA-cation for the delaminated SNT. The two peroxide-modified materials do not have significant differences by any of these characterization methods. As with all peroxide-modified titanates, these peroxide-modified materials exhibit a yellow color, see **figure 8a**. **Figure 8** also shows TEM images of a typical delaminated titanate material **(b)** and also the colloidal TiO_2 obtained by Turbula®-treatment **(c)**. Both are sufficiently small size and high surface area to provide a stable colloid as shown in **8a**. By TEM, differences between the SNT derived materials and Cs-titanate derived materials are subtle. The SNT-derived materials are 'wispier'. We see more significant differences via AFM, and this is discussed later. The colloidal TiO_2 obtained via Turbula processing of Degussa P25 TiO_2 is 20-80 nm diameter.

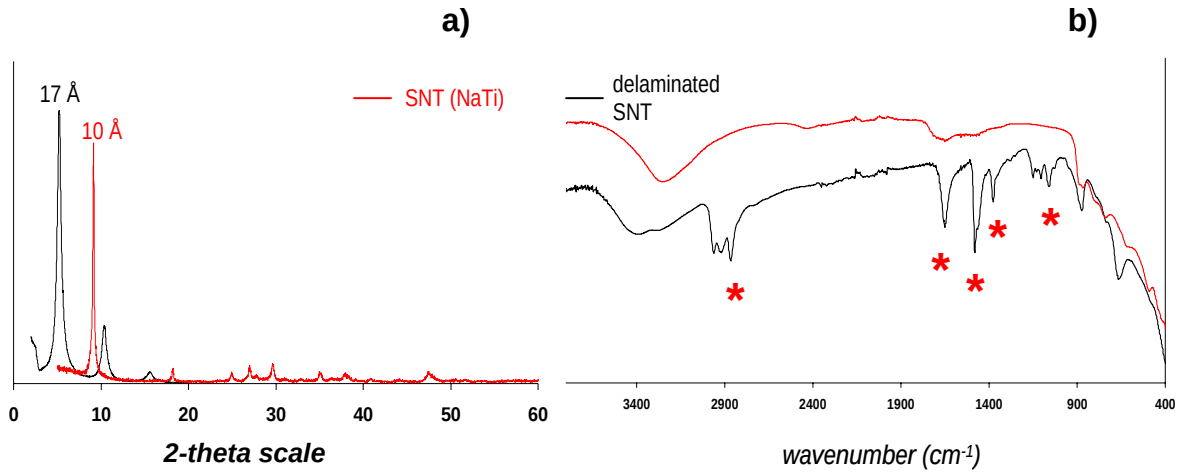

Figure 7. Powder X-ray diffraction (a) and infrared (b) spectra of NaTi (SNT) and NaTi delaminated with TBA-OH (tetrabutylammonium hydroxide). Stars for the infrared spectrum of delaminated NaTi denote the TBA cation.

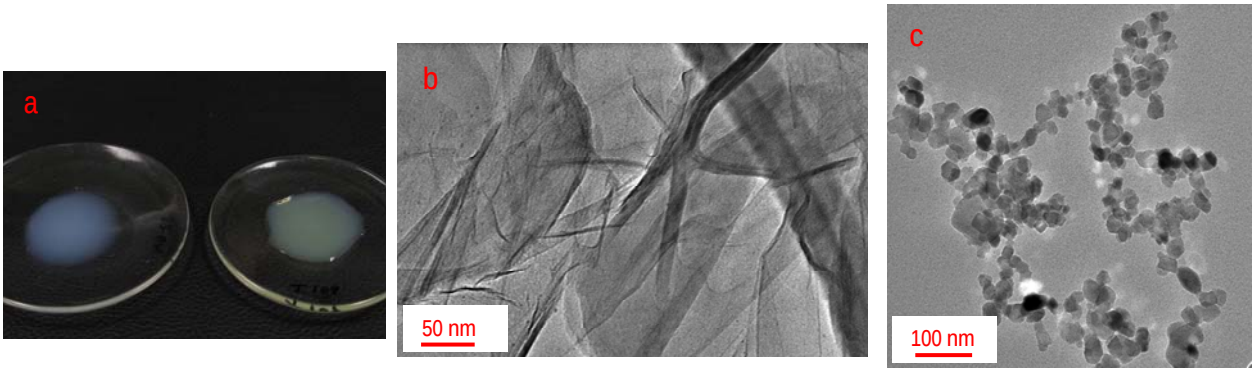

Figure 8. a. photograph of aqueous colloid of delaminated titanate (white) and peroxide-titanate (yellow). **b**. TEM image of typical delaminated titanate. **c**. TEM image of colloidal Degussa P25™ TiO_2 obtained from Turbula processing (see text).

We found that NaTi and CsTi derived materials were very similar in their characteristics, including photocatalytic behavior (see below). However, the distinct advantage of the NaTi is

the easier preparation. While CsTi involves two mixing and heating steps for the initial synthesis, the NaTi is just one simple step (see Experimental). More importantly, the exchange of H^+ for the alkali, which is imperative for subsequent delamination with TBA-OH, occurs much more readily for NaTi. Complete proton exchange of CsTi was originally reported to require 3 x 24 hr exchange steps.(17, 18) With use of the Turbula®, we were able to completely the exchange in 2 hr exchange steps; yet three separate steps of providing fresh 1M acid solution was still necessary. On the other hand, H^+ exchange of NaTi was complete in a single 2 hr contact time with 1M acid solution. This is a distinct advantage for both research and industrial applications. The obvious difference is the Cs in CsTi is not hydrated, whereas the Na in NaTi is hydrated in the parent material; and thus the hydrated ion is more readily mobilized in the aqueous environment.

Methyl-orange photodegradation via delaminated titanates. Testing of the photocatalytic capacities of the delaminated titanates was initiated in the methyl orange, pH 4.7 to 5.0 system, using stable colloidal suspensions without the need of stirring over the 60 or 90-minute duration of UV exposures. The use of multi-well plates allowed the controlled comparison of several materials in a single session or the periodic withdrawal of samples from replicate wells without disturbance to the remainder. The ultraviolet light field previously was found to be suitably uniform using two mapping experiments that distributed 5-mL portions of a uniform titanate/MO mixture into 12 wells. Readings at 590 nm after 90 minutes exposure resulted in an average MO depletion of 2.82×10^{-5} mol/L/hr, with a standard deviation of 0.036, or relative standard deviation of only 1.3%.

At a concentration of 50 µg mL^{-1} in MO, photocatalytic oxidation rates of Cs-titanate and SNT-derived candidates, whether peroxide-treated or not, were close to one another (**Figure 9**), with all achieving the decomposition of at least 6.7×10^{-5} mol/L (67%) in one hour. Consistent functional differences between the four materials were resolved only upon moderating conditions to make the test system more sensitive: energy input was reduced by moving the plates from 18 cm to 26 cm from the UV source; the starting dye concentration was reduced from 1.0×10^{-4} M to 5.0×10^{-5} M; and testing was done to determine optimal concentrations of the titanate nanosheets and a Degussa P25 TiO_2 control. The original 50 µg mL^{-1} proved to be too high, presumably because the blockage of light penetration into the liquid overcomes the advantage of increased catalytic surface area as the titanate concentration increases. Although exact doses do not appear to be critical, **Figure 10** shows that the titanate nanosheets all achieved optimum efficacy at approximately 20 µg mL^{-1} while P25 performed best at 40 µg mL^{-1} but was less sensitive to concentration changes.

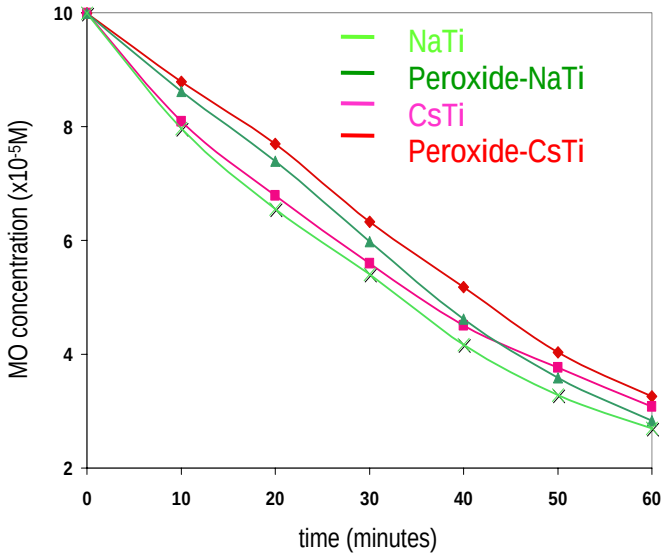

Figure 9. Photocatalytic oxidation of methyl orange by delaminated titanates with catalyst concentration of 50 μg ml^{-1}. Differences in activity between the four materials was not significant under these conditions.

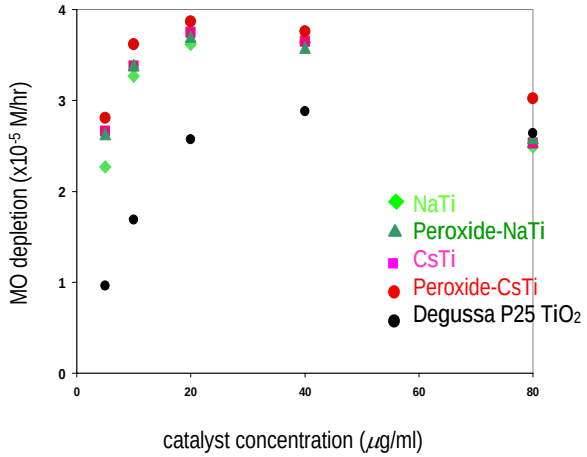

Figure 10. Photocatalytic degradation of methyl orange by delaminated titanates and Degussa P25™ TiO_2 as a function of catalyst concentration. Differences between the delaminated titanates were not significant at most points, but differences between their activity rates from one concentration to the next were significant (Student's t-test, $P < 0.05$, N=4) except between 20 and 40 µg/ml, as were the activity differences for TiO_2, except between 60 and 80 µg/ml.

Performance differences between the titanates became apparent when they were used at suboptimal concentrations. Peroxide-treated versions of both SNT and Cs-titanate-derived catalysts routinely exhibited a modest advantage (2 - 19% oxidation rate improvement), as exemplified in **figures 11a** and **b**. Small variations in the relative performance difference were chiefly due to aging of the suspensions, as the peroxide-treated materials tended to form microaggregates over a period of several weeks at a faster rate than their untreated counterparts.

There was no consistent difference in the photocatalytic efficiency of the SNT versus the Cs-titanate-derived delaminated catalysts. However, as discussed above, the distinct advantage of the SNT is derived from the ease of preparation.

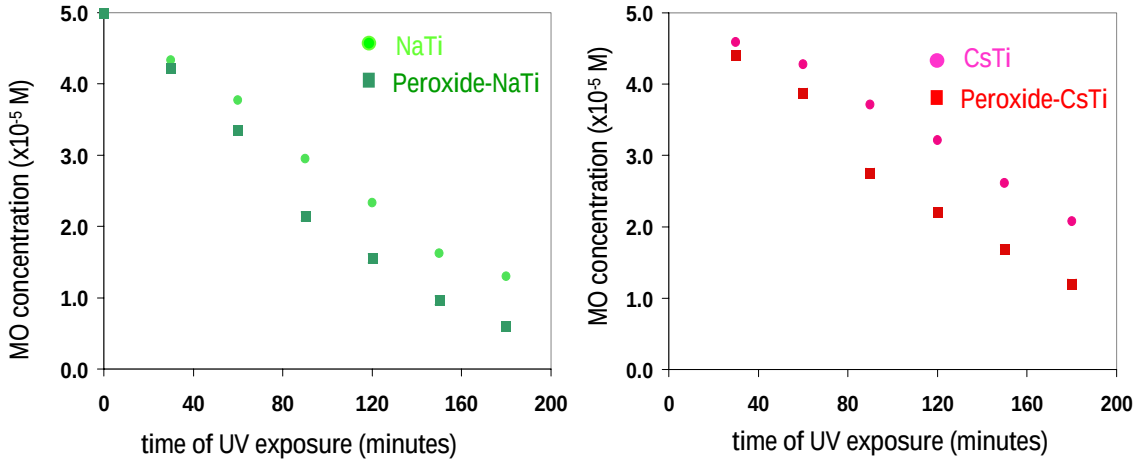

Figure 11. Comparing the performance of delaminated titanates, with and without peroxide treatment. Titanate catalyst concentration is 5 μg/ml. Resulting concentration ranges for MO were $\leq 0.2 \times 10^{-5}$ M at each point (N = 3), and $P < 0.05$ after 60 minutes for peroxide-nonperoxide comparisons in both the NaTi- and CsTi-derived materials.

Bromophenol-blue photodegradation via delaminated titanates. Methyl orange provides a convenient testing system, but is limited to a narrow range of acidic pH in which its color is stable. If the usefulness of photocatalysts is to include oxidative destruction of environmental contaminants, they must be efficacious at a higher pH, generally 7-9. Another organic dye, bromophenol blue (BrB) was selected because its absorbance spectrum is essentially stable between pH 6 and 9, a range conforming with most natural water sources. A useful attribute of BrB that we have discovered is its reproducible, linear rate of photodegradation when exposed to UV light in the absence of any catalyst (**figure 12**). And so, a UV-exposed standard BrB without titanates was used as an indicator of total irradiation from one experiment to the next. For all data from the BrB testing system, the amount of uncatalyzed photodegradation (UPD) measured in each experiment was subtracted as appropriate to calculate the net effect of the photocatalysts.

Photocatalysis of BrB in the pH range from 6.0 to 9.0 (in 5 mM sodium borate), in one unit intervals, was surveyed using delaminated NaTi and Degussa P25 ™ TiO_2. The effect of pH change was significant (**figure 13**). Both catalysts demonstrated the least activity at neutrality and had improved rates at both higher and lower pH. The changes in the rate of catalysis shown here were not associated with flocculation, which has been observed to be a limiting factor in more concentrated, alkaline buffers. The natural UPD rate did not change significantly in connection with pH.

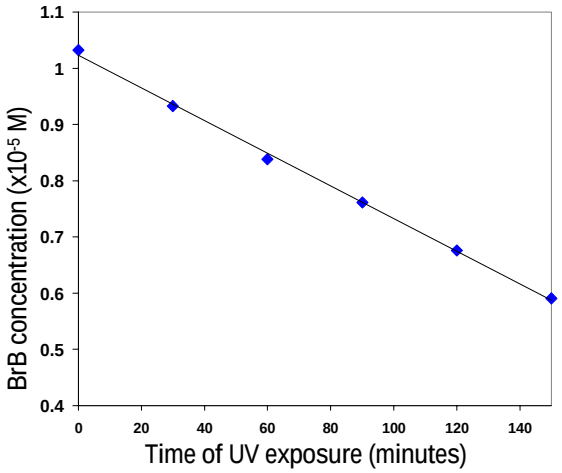

Figure 12. Natural photodegradation of bromophenol blue without a catalyst over time at 26 cm from the UV light source.

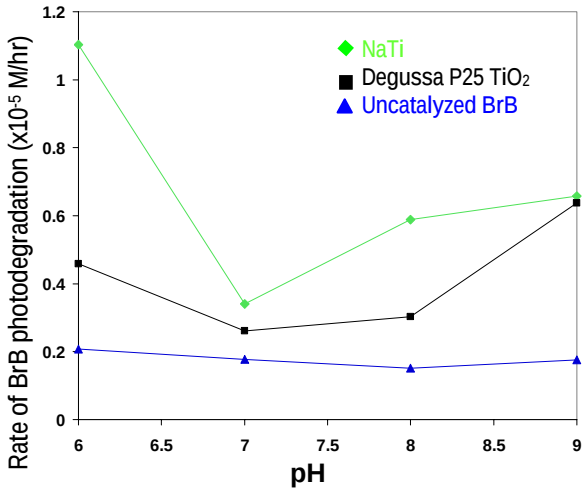

Figure 13. Effect of pH in 5 mM Na borate on one-hour photo-catalytic degradation of bromophenol blue by SNT-derived delaminated titanate compared with TiO_2 and uncatalyzed photodegradation under UV. (Triplicate values varied within ± 0.014 x 10^{-5} M/hr from mean at each point.)

In shifting the testing program from an acidic to a pH 8 environment, different buffers were evaluated. In an experiment that compared 5 mM sodium phosphate, sodium bicarbonate, and sodium borate buffers at pH 8.0±0.1, the depletion of BrB by delaminated titanate catalysis appeared to be enhanced in the phosphate by about 28 percent (with N=4, NaTi catalyst depleted BrB an average of 51.5±2.5% in borate and bicarbonate vs. 66±1% in phosphate in one hour) while this effect was not seen in TiO_2. Several experiments were performed to confirm this phenomenon occurring for both the sodium- and cesium-derived catalysts, including an escalation of the phosphate content of 5 mM sodium bicarbonate buffer with the pH constant at 8.0 (**Figure 14**). This resulted in a clear dose effect, while no such trend appeared in degradation of BrB without catalyst, exposed to UV light in the same buffer series.

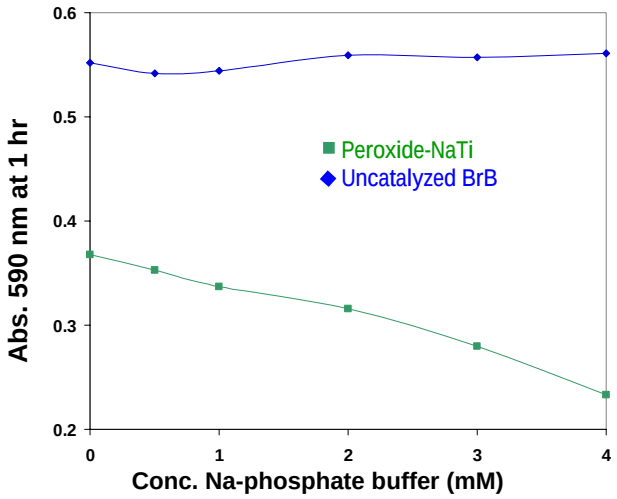

Figure 14. Effect of escalating level of phosphate buffer on photocatalytic degradation of BrB compared with uncatalyzed photo-degradation, with all data points at one hour of UV exposure. Lower absorbance indicates a faster rate of depletion. (Triplicate values varied within ± 0.010 AU of mean at each point.)

UV-Vis characterization of titanate photocatalysts. Characterization of the different delaminated titanates via standard techniques such as X-ray diffraction, infrared spectroscopy and various microscopies (TEM, AFM, SEM) did not reveal obvious differences between the materials that we could link to variations in catalytic efficacy. UV-vis spectroscopy, measuring the adsorption bandgap energy, seemed the most sensitive technique in detecting differences between materials. In **figure 10**, we show the UV-vis spectra for delaminated titanates NaTi, peroxide-NaTi, CsTi, peroxide CsTi and phosphate-treated NaTi. The peak adsorption is very similar for NaTi, CsTi, peroxide-NaTi and peroxide-CsTi. The major difference however is the NaTi and peroxide-NaTi materials both have a broader shoulder into the visible wavelengths and decreased intensity; peroxide-NaTi in particular. Since these materials all have similar photocatalytic behavior for MO degradation, this suggests it is the peak adsorption that is important; where the UV source we utilize emits at 254 nm. However, this is a strong indication of structural differences between the titanate layers derived from SNT and from Cs-titanate; most likely in Ti-vacancy or defect concentration. The phosphate-treated peroxide-NaTi has a maximum adsorption at 260 nm, as well as a broader shoulder towards lower wavelength and, therefore, the bandgap is better matched to the UV source. This may explain the enhanced performance, although we have not been able to discern distinct structural, morphological, or compositional changes that accompany this enhanced performance. Although the Degussa P25 TiO_2 is a poorer catalyst than all of the delaminated titanates, it also has an adsorption maximum at 261 nm (see **figure 15**); which is not consistent with our interpretation of the enhanced performance of phosphate-treated peroxide-NaTi. However, TiO_2 it is a different material with lower surface area; so a direct comparison is not meaningful. [Note: The term 'surface area' in this context simply describes the geometrical differences between a sheet and a sphere: a sheet has higher surface:volume ratio. No surface areas have actually been measured since the

photocatalysis takes place in an aqueous colloid; and the necessity to perform these measurements on dried material renders the measurements meaningless.]

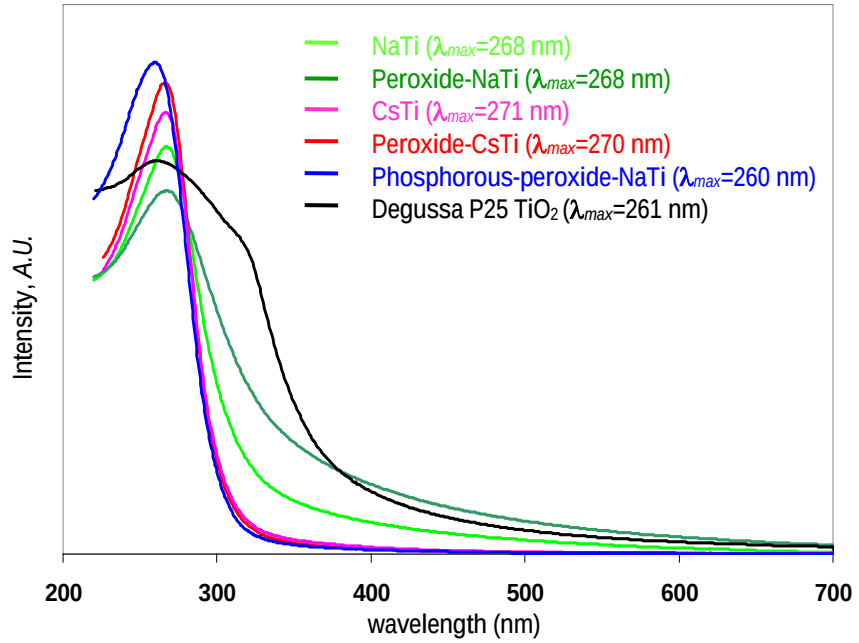

Figure 15. UV-vis spectra of aqueous suspensions of the delaminated titanate photocatalysts, Degussa P25™ TiO_2, and phosphate-modified delaminated titanate. Adsorption maxima (nm) for each phase is in parenthesis.

Two recent studies revealed that ~1% phosphorous-doping of TiO_2 and mesoporous TiO_2 improved photocatalytic activity, presumably by increasing surface area and creating surface traps to delay e^-/h^+ recombination.(31, 32) We did not see this same enhancement effect with Degussa P25 TiO_2. However, the method of introduction of the phosphorous to the titanate materials was very different between these prior reports and our experiments. In the prior experiments, the phosphate was introduced before forming the TiO_2 via calcination. We introduce it only in the aqueous phase, so it would be incorporated into the delaminated titanates via surface adsorption or reaction with the surface. The surface of layered titanates is likely more reactive towards phosphate adsorption/reactivity than the TiO_2.

Finally, the broad shoulder towards the visible wavelengths of the NaTi and peroxide-NaTi spectra indicate these materials may be more effective for photocatalysis compared to the CsTi materials, if a longer wavelength source was utilized in the application.

3.4 Summary

Sodium nonatitanate-derived delaminated nanosheets are comparable in photocatalytic activity with Cs-titanate-derived catalysts. This is probably because the construction of the layers, edge-sharing TiO_6 octahedra is similar for the two materials. While the Cs-titanate structure has been

reported, the structure of SNT has never been investigated in-depth and is the focus of current study. The SNT-derived materials are very attractive for further development, since both their initial synthesis and processing is much simpler: From initial synthesis to final delamination, SNT requires ~3 processing steps compared to 7-9 steps for Cs-titanate. The primary differences are in the initial synthesis and the acidification prior to delamination. Furthermore, sodium is much less costly than cesium. Since SNT is synthesized hydrothermally and Cs-titanate is synthesized via solid-state processing, both have advantages and disadvantages for chemical modifications such as by doping with other elements to enhance activity, selectivity, or shift the absorption band-gap. Both forms were shown to be superior to standard TiO_2 when tested as colloidal suspensions under a germicidal UV light. This is probably a combined effect of higher surface area and a shifted bandgap that provides a better match with the UV-source.

Further treatment of these preparations with hydrogen peroxide appears to confer some degree of enhancement in most photodegradation experiments. Treatment with millimolar concentrations of sodium phosphate was seen to accelerate photocatalysis by the delaminated titanates rather significantly. These findings offer some new possibilities of simple chemical modifications to enhance photocatalytic activity. Furthermore, the ubiquity of phosphate in common environmental conditions and some contaminants as well suggest this needs to be considered as we continue to characterize these materials for their use in water treatment applications.

This page is intentionally left blank

4 THE COMPLETE FUNCTIONALIZED SURFACE

4.1 Overview

In this section, we discuss assembly and function of the entire 'package'. These were assembled on mica surfaces, chosen for their pristine and atomically flat nature that is necessary for Atomic Force Microscopy (AFM) surface imaging and adhesion studies. Refer to **figure 16** for the discussion below. The cationic function group of choice from Chapter 2 of this report, the $[GaO_4Al_{12}(OH)_{24}(H_2O)_{12}]^{7+}$ polycation was utilized to both adhere the titanate sheets to the mica surfaces, as well as provide an electrostatically attractive surface for the microorganism such as MS2 bacteriophage. Therefore, a cation-anion-cation multilayered sandwich is assembled on the mica, see **figure 16**.

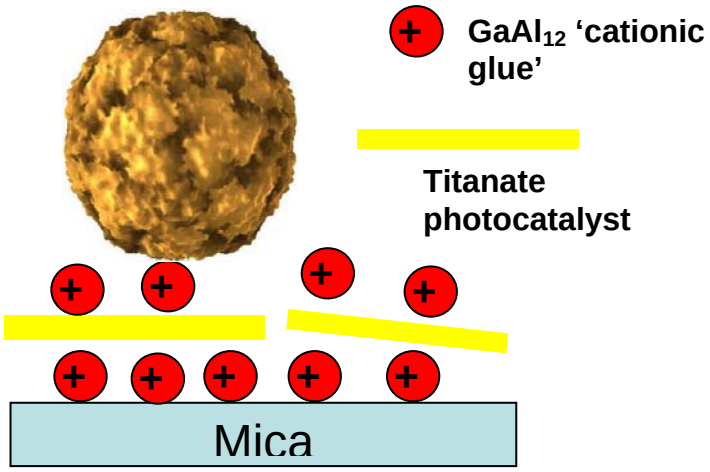

Figure 16. Cartoon of assembly of functional surface on mica, for binding a microorganism and photocatalytically destroying the adsorbed specie.

In this section, we demonstrate that the photocatalysts remain active in the surface adsorbed state. We image MS2 adsorbed to 1) $GaAl_{12}$ polycation only, and 2) $GaAl_{12}$-titanate-$GaAl_{12}$. In the latter scenario, we demonstrate photocatalytic destruction of the phage as well.

4.2 Experimental

Preparation and photocatalysis of surface-bound titanates. Other experiments were designed to determine whether delaminated titanates could be bound to a solid surface and retain photocatalytic ability. To this end, Cs- and Na-derived, delaminated titanates were bound to freshly-exposed muscovite mica (Ted Pella) surfaces that had been previously coated with $[GaO_4Al_{12}(OH)_{24}(H_2O)_{12}]^{7+}$ polycations, denoted $GaAl_{12}$, synthesized as described prior.(33) Four 1-inch square mica pieces coated only with $GaAl_{12}$ (at 1 mg/mL in deionized water, with

five minutes contact) and four with $GaAl_{12}$ followed by a coating with the titanate were rinsed thoroughly with deionized water and dried at room temperature. Each piece was placed beneath 0.5 mL of $2.5x10^{-5}$ M MO and exposed to UV light for three hours, after which all of each MO load was recovered with limited rinsing, the final volumes equalized, and their absorbance was read to determine the amount of dye remaining.

Although several procedures and conditions were employed experimentally, the most successful protocol for adsorbing MS2 viruses to mica was the following. Mica (Ted Pella, Hi-Grade) was cleaved with a new scalpel blade and immediately immersed in $GaAl_{12}$ (1000 ppm Al, pH 4.5 in water) for 10 minutes, then rinsed with purified water and allowed to dry. Subsequent coatings were achieved by applying the desired solution or suspension dropwise to the upper, newly cleaved and treated surface for a total of 0.5 mL on a 1-inch square of mica. After ten minutes, the liquid was aspirated from the mica, which was then rinsed with purified water and allowed to dry.

MS2 virus solutions used for coating were assayed at 0.2 to 1.0 x 10^{10} viable pfu/mL in 0.01 M phosphate buffer, pH 6. However, due to the serial subculturing used to generate the virus stock and the natural attrition rate of MS2, it is likely that viable viruses were greatly outnumbered by noninfectious capsids. For adsorbing MS2 onto titanate sheets, the delaminated titanate was applied to mica first, than counter-coated using a second treatment with $GaAl_{12}$. After ten minutes, unbound $GaAl_{12}$ was rinsed off, and MS2 solution was applied dropwise as described

AFM. Tapping mode atomic force microscopy (**AFM**) using a Veeco Dimension 5000 Tool was used to examine surface-adhered titanate layers and MS2 adsorbed onto cleaved mica surfaces. With this AFM the mica substrate root mean square roughness was measured at 50 pm in a 1 um scanned area, indicating a noise floor for the system. Height and distance calibration was verified using standard calibration samples

4.3 Results and Discussion

The use of colloidal suspensions of the titanate nanosheets is convenient for screening experiments utilizing different materials, conditions and contaminants; but surface-bound titanates have greater potential for practical use in remediating organic and microbial contamination in water. Furthermore, the delaminated titanate layers have the ideal morphology for adsorption onto a flat surface. Coupling agents were explored for the purpose of affixing the nanosheets to high-quality mica surfaces (specifically for AFM characterization). The titanate layers are anionic under most pH conditions, and therefore we considered cations that would adhere readily to the anionic mica surface when deposited from an aqueous solution. While organic cations can be utilized (polymers for instance(21)), they might themselves be vulnerable to catalytic photo-oxidation. Therefore we first explored inorganic polycations. Use of the aluminum tridecamer $[AlO_4Al_{12}(OH)_{24}(H_2O)_{12}]^{7+}$ (Al_{13}) has in fact been reported for exactly this purpose.(34) However, prior studies have shown that the related Ga-centered aluminum cluster, $[GaO_4Al_{12}(OH)_{24}(H_2O)_{12}]^{7+}$, $GaAl_{12}$ is more stable and carries a higher charge in aqueous solution,(1) so we opted to utilize this 'cationic glue' instead.

Dense coverages of delaminated titanate from both CsTi and NaTi, as well as the peroxide derivatives, were assembled on $GaAl_{12}$-coated mica surfaces. Typical CsTi and NaTi coatings imaged by AFM are shown in **figure 17a** and **b**, respectively. Morphologies differences are apparent. Qualitatively, the CsTi derived coatings are more sheet-like, whereas the NaTi layers can be described as more fibrous. Two profiles are shown for each image; the CsTi layers and the NaTi layers. The maximum height difference is 4 nm for both the CsTi and NaTi layers. The double-layer of edge-sharing TiO_6 octahedra of the Cs-titanate phase is ~0.4nm thick;(17) and the GaA_{12} polycation is ~1 nm in diameter. We assume the titanate layers of SNT have similar structure, and a corresponding similar thickness. Therefore, the dense layers shown in **17a&b** are fewer are than 10 titania-layers thick. It is not clear from these studies if TBA resides between some co-adsorbed titania layers. If the mica is immersed in a delaminated titanate colloid *without* pretreatment with the polycation, we observe by AFM imaging only a very sparse coating, see **figure 18** (CsTi-derived layers). This study allowed the measurement of a single adsorbed titanate layer; ~ 1nm. This is approximately twice the thickness of the double-layer of TiO_6 octahedra of the Cs titanate structure. However, in this case where there is no pre-treatment with $GaAl_{12}$, it is likely that some TBA-cations are co-adsorbed between the mica and the titanate layer.

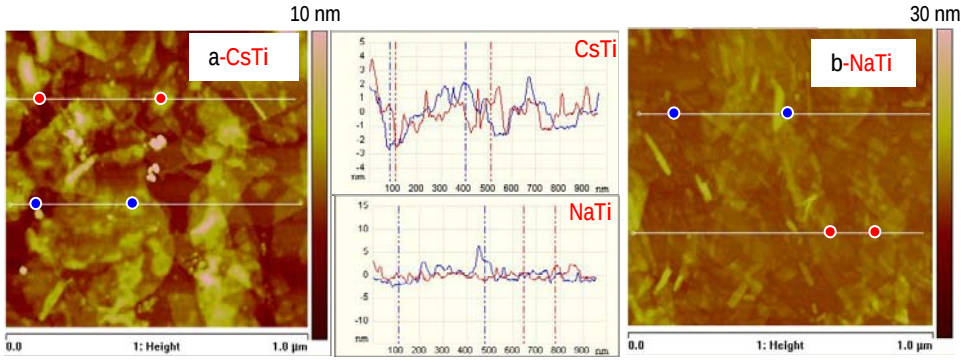

Figure 17 a & b. AFM images of delaminated layers derived from Cs titanate (left) and SNT (right). Mica surfaces are pre-treated with $GaAl_{12}$ polycation. Height profiles for each across the sections denoted by red and blue circles are shown in the center panel of the figure.

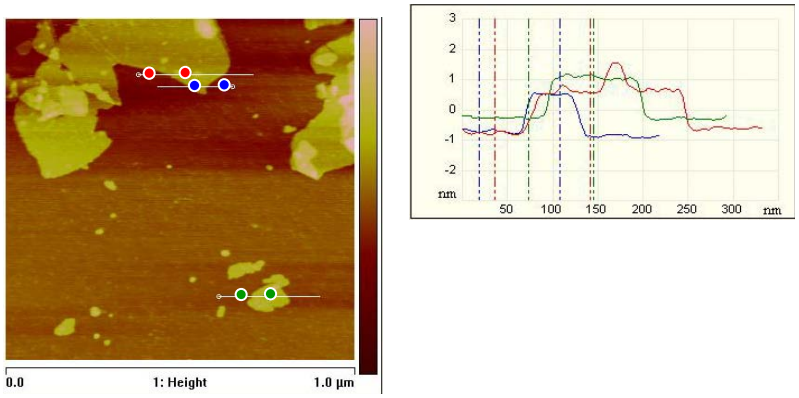

Figure 18. Left—AFM image of Cs-titanate layers adsorbed onto mica with pretreatment with $GaAl_{12}$. Red, blue and green circles denote cross sections cross sections shown in the height profile (right).

Photocatalytic degradation of methyl-orange utilizing layers derived from SNT affixed on mica surfaces demonstrated these catalysts are also functional in this form. Average remaining concentration of MO after the first UV exposure of the solid-phase catalyst squares was $0.16x10^{-5}$ M as oppose to the control squares with $1.30x10^{-5}$ M MO remaining, a reduction of 88% for three hours exposure time. We also demonstrated the photocatalytic activity of Degussa P25 TiO_2 for comparison and these are compared in **figure 19**. The TiO_2 nanoparticles reduced the MO concentration to around 56%, again demonstrating the superior performance of the titanate nanosheets. The same mica pieces were rinsed off with deionized water, dried overnight, and used the next day in a repeat experiment. In the second trial of the same surfaces without additional coating, the remaining MO concentration recovered from the titanate squares was $0.14x10^{-5}$ M as oppose to the control squares with $1.29x10^{-5}$ M MO remaining, a reduction of 89%, again over three hours. There is no loss in photocatalytic activity, demonstrating the robust nature of these materials, and the appropriate choice of an inorganic 'glue' to bind the anionic titanate layers to the anionic substrate. Although mica was chosen to optimize conditions for AFM imaging, most filtration substrates or media are in fact anionic, so the inorganic polycation is important for more practical applications as well.

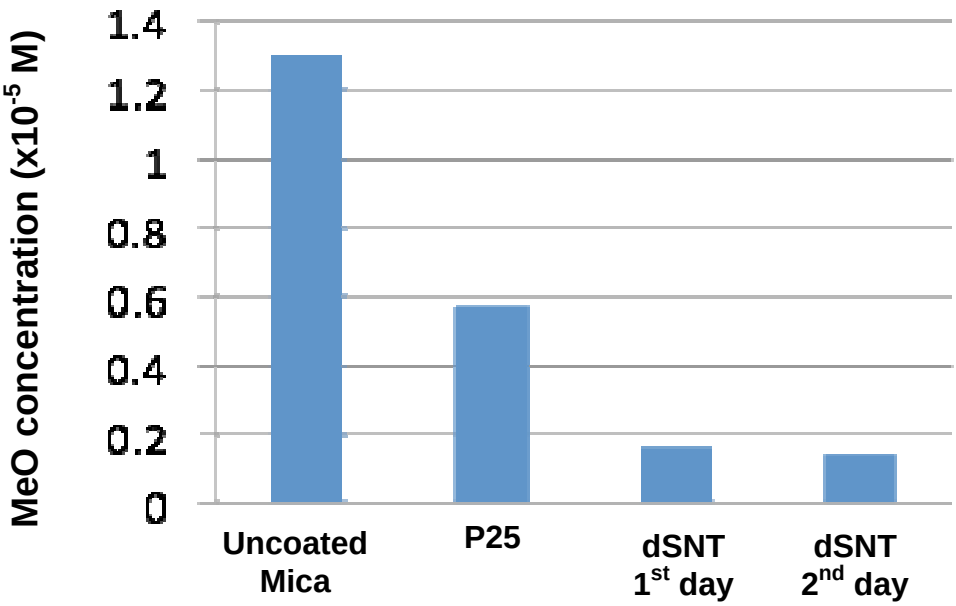

Figure 19. Comparing the photocatalytic activity via methyl orange degradation of Degussa P25 TiO_2 and titanate nanosheets, both adsorbed onto mica substrates. Also demonstrates retention of activity upon reuse for the titanate nanosheets.

In **figure 20**, we have captured an image of the MS2 adsorbed onto a mica surface treated with $GaAl_{12}$ polycation only. The MS2 phage has a diameter of 27 nm. Here we observe 'flattened' phage bodies, with a height above the mica of 12-15 nm and a width, parallel to the surface of around 40 nm. This suggests the adherence to the cationic surface is quite strong. **Figure 21** shows the MS2 adsorbed onto a surface that has been functionalized with a $GaAl_{12}$-titanate-$GaAl_{12}$ multi-layer before (top) and after (bottom) photocatalysis. The photocatalytic activity of the titanate sheets destroyed the phage within 30 minutes of UV-irradiation.

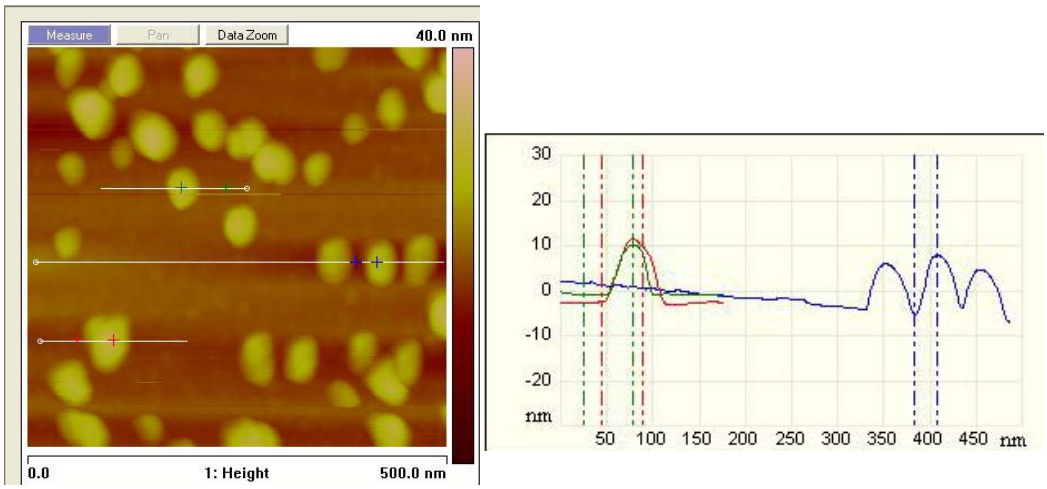

Pair	Horizontal Dist.	Vertical Dist.	Surface Dist.
0	25.440 (nm)	12.940 (nm)	29.678 (nm)
1	44.031 (nm)	12.312 (nm)	47.528 (nm)
2	53.816 (nm)	11.024 (nm)	56.566 (nm)

Figure 20. MS2 adsorbed onto mica functionalized with $GaAl_{12}$ polycation (top left). Top right shows profile scans of the MS2, and the horizontal and vertical distances are listed on the bottom—the colored crosses on the picture mark the corresponding colored profile trace and height and width listed in the table on the bottom.

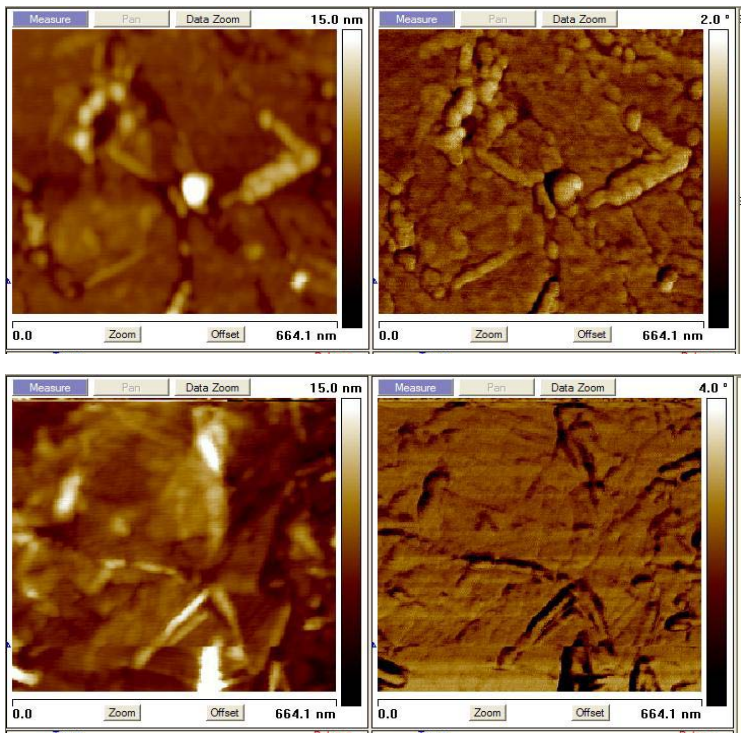

5 SUMMARY AND OUTLOOK

This study showed that we can functionalize ideal surfaces with 1) chemical species that bind microorganisms and 2) photocatalysts that are of ideal geometry (flat) and chemistry (anionic) for compatibility with the binding chemical species. We determined that a high cationic charge is important for adsorbing the microorgansms by chemical affinity (rather than settling or some other physical mechanism). Hydrophobicity is also potentially important, but it can degrade under UV-irradiation for photocatalysis. Future work in this thrust may involve functionalizing membranes for water filtration, to improve filtration beyond size exclusion, into the chemical affinity realm. The titanate layers alone may also be useful for antifouling; which is one of the biggest challenges of water treatment by filtration.

In the process of these studies, we also discovered that the delaminated titanates are very effective for selectively precipitating rare-earth metals out of solution. Rare-earth metals (RE) are used extensively in hybrid vehicles, wind turbines, 'supermagnets' and display and lighting applications. Given the current shortage of rare-earths on the global market (due to China withholding their supply), issues around mining, separating and recycling rare-earths have become exceedingly important. Sorption and precipitation of rare-earths may be applied in recycling of rare-earths, cleaning mine drainage, and other mining separation processes. **Figure 22** shows the adsorption of Eu from solution via delaminated titanates as a function of amount of Eu in solution, to determine a 'breakthrough curve'. Given an approximate formulae of $[TBA]_3[Ti_3O_{7.5}]\cdot 3H_2O$ (TBA=tetrabutylammonium), the delaminated titanates can theoretically adsorb 17 wt% RE, Eu and in this example, 10 wt% Eu is adsorbed. **Figure 23** shows the delaminated titanate and the Eu-exchanged titanate under a UV-lamp, showing the red glow from Eu. We also determined the titanate layers can be recycled for reuse. The Eu can be removed with acid, delaminated again, and reused for Eu sorption. This cycle is summarized in the equation below:

$$[TBA]_3[Ti_3O_{7.5}]\cdot 3H_2O \rightarrow Eu^{3+} \rightarrow [Eu][Ti_3O_{7.5}]\cdot 3H_2O \rightarrow 3H^{+} \rightarrow [H]_3[Ti_3O_{7.5}]\cdot 3H_2O$$

$$\rightarrow 3TBA^{+} \rightarrow [TBA]_3[Ti_3O_{7.5}]\cdot 3H_2O$$

Another salient point of these studies is in a solution with sodium as a competitive ion (200:1 Na:Eu ratio), the Eu is removed selectively: 92% of the Eu is removed.

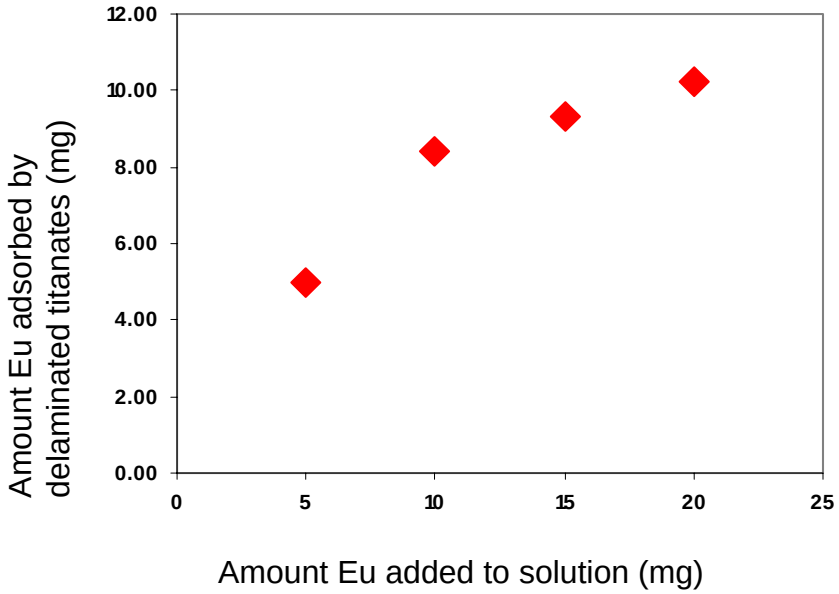

Figure 22. Removal of Eu from aqueous solution (35 ml) via 100 g delaminated titanate, as a function of Eu concentration in the solution. A maximum of 10 wt% Eu is adsorbed by the delaminated titanate.

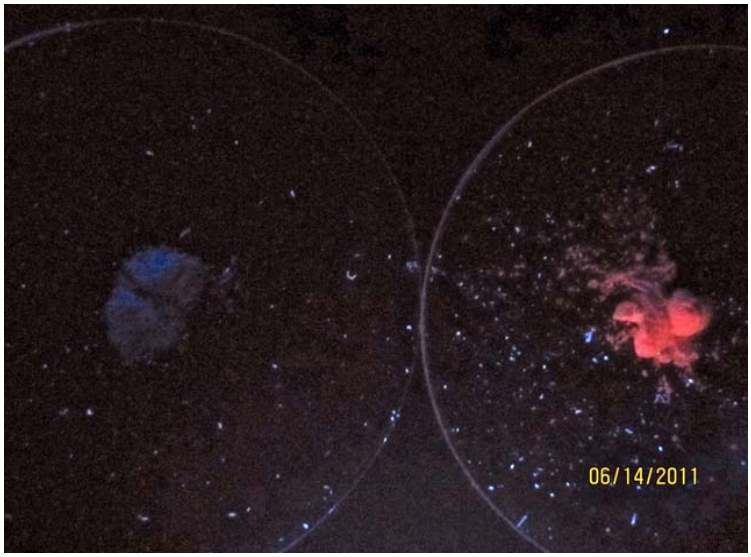

Figure 23. $[TBA]_3[Ti_3O_{7.5}]\cdot 3H_2O$ (left) and $[Eu][Ti_3O_{7.5}]\cdot 3H_2O$ (right) illuminated by a UV lamp, showing the red glow from Eu^{3+}.

6 REFERENCES

1. Stewart, T.A., Trudell; D.E., Alam, T.M.; Ohlin, C.A.; Lawler C.; Casey, W.H., et al. "Enhanced Water Purification: A Single Atom Makes a Difference." *Environ Sci Technol*. **2009**; 43(14): 5416-22. doi: Doi 10.1021/Es803683t.

2. Williams, F.P., Stetler, R.E., Safferman, R.S. "USEPA Manual of Methods for Virology." Washington, DC: U.S. Environmental Protection Agency; **2001**.

3. Wang, Z.L., Ma, Y., Zhang, R.L., Xu, D., Fu, H.B., Yao, J.N. "Fabrication of self-assembled ultrathin photochromic films containing mixed-addenda polyoxometalates $H_5PMo_{10}V_2O_{40}$ and 1,10-decanediamine." *J Solid State Chem.* **2009**; 182(4): 983-8. doi: 10.1016/j.jssc.2009.01.014.

4. Fujishima, A; Honda K.; "Electrochemical Photolysis of Water at a Semiconductor Electrode." *Nature*. **1972**; 238: 37-8.

5. Mills, A; Davies R.H; Worsley D. "Water Purification by Semiconductor Photocatalysis." *Chem Soc Rev*. **1993**: 417-25.

6. Gratzel M. "Artificial Photosynthesis: Water cleavage into Hydrogen and Oxygen by visible light." *Acc Chem Res*. **1981**; 14: 376-84.

7. Carp O; Huisman C.L; Reller, A. "Photoinduced reactivity of titanium dioxide." *Progress in Solid State Chemistry*. **2004**; 32: 33-177.

8. Kudo, A; Miseki, Y. "Heterogeneous photocatalyst materials for water splitting." *Chem Soc Rev*. **2009**; 38: 253-78.

9. Osterloh, F.E. "Inorganic Materials as Catalysts for Photochemical Splitting of Water." *Chem Mater*. **2008**; 20: 35-54.

10. Liu, G; Wang, L; Sun, C; Yan, X; Wang, X; Chen, Z; et al. "Band to band visible light photon excitation and photoactivity induced by homogeneous nitrogen doping in layered titanates." *Chem Mater*. **2009**; 21: 1266-74.

11. Ni, M; Leung, M.K.H; Leung, D.Y.C.; Sumathy, K. "A review and recent developments in photocatalytic water-splitting using TiO_2 for hydrogen production." *Renewable & Sustainable Energy Reviews*. **2007**; 11(3): 401-25.

12. Bavykin, D.V; Walsh, F.C. "Elongated Titanate Nanostructures and their applications." *Eur J Inorg Chem.* **2009**: 977-97.

13. Mor, G.K; Varghese, O.K; Paulose, M; Shankar, K; Grimes C.A. "A review on highly ordered vertically oriented TiO_2 nanotube arrays: fabrication, material properties and solar energy applications." *Solar Energy Materials and Solar Cells*. **2006**; 90(14): 2011-75.

14. Anpo, M; Takeuchi, M; "The design and development of highly reactive titanium oxide photocatalysts operating under visible light irradiation." *Journal of Catalysis*. **2003**; 216: 505-16.

15. Sasaki T, Watanabe M. Osmotic Swelling to Exfoliation. Exceptionally high degrees of hydratoin of a layered titanate. J Am Chem Soc. 1998;120:4682-9.

16. Grey IE, Madsen IC, Watts JA. Cs-titanate structure. J Solid State Chem. 1987;66(1):7-19.

17. Sasaki, T; Watanabe, M; Michiue, Y; Komatsu, Y; Izumi, F; Takenouchi, S. "Preparation and acid-base properties of a protonated titanate with the lipidocrocite-like layer structure." *Chem Mater*. **1995**; 7(5): 1001-7.

18. Sasaki, T; Komatsu, Y; Fujiki, Y. "A new layered hydrous titanium dioxide H_xTiO-H_2O." *J Chem Soc, Chem Commun*. **1991**: 817-8.

19. Sasaki, N; Ebina, Y; Takada, K; Sasaki, T. "Electronic Band structure of titania semiconductor nanosheets revealed by electrochemical and photoelectrochemical studies." *J Am Chem Soc*. **2004**; 126(18): 5851-8.

20. Sasaki, T., Ebina, Y; Watanabe, M; Decher, G. "Multilayer ultrathin films of molecular titania nanosheets showing highly efficient UV-light absorption." *Chem Comm*. **2000**: 2163-4.

21. Sasaki, T; Ebina, Y; Tanaka, T; Harada, M; Watanabe, M. "Layer-by-layer assembly of titania nanosheet/polycation composite films." *Chem Mater*. **2001**; 13(12): 4661-7.

22. Shibata, T; Sakai, N; Fukuda, K; Ebina, Y; Sasaki, T. "Photocatalytic properties of titania nanostructured films fabricated from titania nanosheets." *Phys Chem Chem Phys*. **2007**; 9: 2413-20.

23. Guo, T; Wang, L; Evans, D.G; Yang, W. "Synthesis and photocatalytic properties of a PAN intercalated layered protonic titanate nanocomposite." *J Phys Chem C*. **2010**; 114: 4765-72.

24. Ide, Y; Nakasato, Y; Ogawa, M. "Molecular Recognitive photocatalysis driven by the selective adsorption on layered titanates." *J Am Chem Soc*. **2010**; 132(10): 3601-4.

25. Kim, T.W; Kim, I.Y; Im J.H; Ha, H.W; Hwang, S.J. „Improved photocatalytic activity and adsorption ability of mesoporous potassium intercalated layered titanate." *J Photochemistry and Photobiology A: Chemistry*. **2009**; 205: 173-8.

26. Allen, M.R; Thibert, A; Sabio, E.M; Browning, N.D; Larsen, D.S; Osterloh, F.E. "Evolution of physical and photocatalytic properties in the layered titanates (A=K,H) and the nanosheets dervied by chemical exfoliation." *Chem Mater*. **2010**; 22(3): 1220-8.

27. Clearfield, A; Lehto, J. "Preparation, Structure, and Ion-Exchange Properties of $Na_4Ti_9O_{20}\cdot xH_2O$." *J Solid State Chem*. **1988**; 73(1): 98-106.

28. Behrens, E.A; Sylvester, P; Clearfield, A. "Assessment of a sodium nonatitanate and pharmacosiderite-type ion exchangers for strontium and cesium removal from DOE waste simulants." *Environ Sci Technol*. **1998**; 32(1): 101-7.

29. Hirakawa, T; Nosaka, Y. "Properties of O_2 and OH formed in TiO_2 aqueous suspensions by photocatalytic reaction and the influence of H_2O_2 and some ions." *Langmuir*. **2002**; 18: 3247-54.

30. Nyman, M; Hobbs, D.T. "A family of peroxo-titanate materials tailored for optimal strontium and actinide sorption." *Chemistry of Materials*. **2006**; 18(26): 6425-35.

31. Zheng, R; Guo, Y; Jin, C; Xie, J; Zhu, Y; Xie, Y. "Novel thermally stable phosphorous-doped TiO_2 photocatalyst synthesized by hydrolysis of $TiCl_4$." *Journal of Molecular Catalysis A: Chemical*. **2010**; 319: 46-51.

32. Fan, X.; Yu, T.; Wang, Y; Zheng, J; Gao, L; Li, Z, et al. "Role of phosphorous in synthesis of phosphated mesoporous TiO_2 photocatalytic materials by EISA method." *Applied Surface Science*. **2008**; 254: 5191-8.

33. Bradley, S; Fyfe, C; Kydd, R; Ronald, A; Kydd, A; Fyfe, C.A. "Characterization of the galloaluminate $GaO_4Al_{12}(OH)_{24}(H_2O)_{12}^{7+}$ polyoxocation by MAS NMR and infrared spectroscopies and powder x-ray diffraction." *Inorg Chem.* **1992**; 31(7): 1181-5.

34. Wang, L; Ebina, Y; Takada, K; Sasaki T. "Ultrathin films and hollow shells with pillared architectures fabricated via LBL self-assembly of titania nanosheets and Keggin ions." *J Phys Chem B.* **2004**; 108: 4283-8.

This page is intentionally left blank.

Internal (Electronic Copy)

1	MS 0359	LDRD office	1911
1	MS 0899	RIM-Reports Management	9536
1	M2497	Central Technical Files	8944

This page is intentionally left blank

Sandia National Laboratories